Author Manuscript

Author Manuscript

Author Manuscript

Author Manuscript

HHS Public Access
Author manuscript
Nat Neurosci. Author manuscript; available in PMC 2010 March 01.

Published in final edited form as:
Nat Neurosci. 2009 September ; 12(9): 1121–1128. doi:10.1038/nn.2368.

Cholinergic modulation of multivesicular release regulates striatal synaptic potency and integration

Michael J. Higley[*], **Gilberto J. Soler-Llavina**[*], and **Bernardo L. Sabatini**
Howard Hughes Medical Institute, Department of Neurobiology, Harvard Medical School, Boston, MA 02115

Abstract

The pleiotropic actions of neuromodulators on pre- and postsynaptic targets present challenges to disentangling the mechanisms underlying regulation of synaptic transmission. Within the striatum, acetylcholine modulates glutamate release via activation of muscarinic receptors (mAchRs), although the consequences for postsynaptic signaling are unclear. Using 2-photon microscopy and glutamate uncaging to examine individual synapses in the rat striatum, we find that glutamatergic afferents exhibit a high degree of multivesicular release (MVR) in the absence of postsynaptic receptor saturation. We show that mAchR activation decreases both the probability of release and the concentration of glutamate in the synaptic cleft. The corresponding decrease in synaptic potency reduces the duration of synaptic potentials and limits temporal summation of afferent inputs. These findings reveal a mechanism by which a combination of basal MVR and low receptor saturation allow the presynaptic actions of a neuromodulator to control the engagement of postsynaptic nonlinearities and regulate synaptic integration.

Introduction

Neuromodulatory systems within the mammalian brain regulate behavioral state, circuit plasticity, and synaptic transmission1. Perturbations of neuromodulators such as acetylcholine (Ach), dopamine, and serotonin contribute to the pathogenesis and treatment of neuropsychiatric disorders including Parkinson's Disease, schizophrenia, and major depression2–5. In contrast to classical neurotransmitters that directly excite or inhibit postsynaptic neurons, neuromodulators generally alter the biochemical state of the neuron, influencing the activities of receptors, ion channels, and signaling cascades. These pleiotropic effects present major technical challenges to elucidating the specific mechanisms underlying neuromodulation of brain function. This difficulty is evident in the striatum, a key component of the basal ganglia necessary for the proper generation of movement that is regulated by neuromodulators such as dopamine and Ach6–8. Ach is released in the striatum by interneurons, and disruption of cholinergic signaling impairs both movement and

Users may view, print, copy, and download text and data-mine the content in such documents, for the purposes of academic research, subject always to the full Conditions of use:http://www.nature.com/authors/editorial_policies/license.html#terms

Correspondence: bsabatini@hms.harvard.edu.
[*]These authors contributed equally to this work.
Author Contributions MJH, GSL, and BLS designed the experiments. MJH and GSL performed the experiments and analyzed the data. MJH and BLS wrote the manuscript.

Author Manuscript Author Manuscript Author Manuscript Author Manuscript

learning of operant conditioning tasks9, 10. Moreover, perturbation of striatal cholinergic signaling contributes to movement disorders including Huntington's and Parkinson's Diseases4, 11, 12.

The majority of cells in the striatum are medium spiny neurons (MSNs) that receive glutamatergic inputs from the cortex and thalamus13, 14. Presynaptic terminals of these afferents express M2-type muscarinic receptors (mAchRs) whose activation reduces the magnitude of synaptic responses in the striatum15–19. MSNs express both M1- and M4-type mAchRs, and ultrastructural analysis has shown that cholinergic terminals are typically apposed to dendritic shafts and spine necks, suggesting that cholinergic receptors may also regulate postsynaptic properties20–22. Previous studies found minimal effects of mAchR activation on postsynaptic glutamatergic currents16, 23 (but see24). Nevertheless, mAchR activation modulates intrinsic membrane properties of MSNs, reducing currents through various voltage-gated Ca and potassium channels25–28. As nonlinear interactions between voltage-sensitive glutamate receptors and other channels can influence synaptic response magnitude and integration29, 30, muscarinic actions on glutamatergic signaling remain unclear.

We studied the modulation of excitatory synapses onto MSNs, combining 2-photon laser scanning microscopy (2PLSM) and 2-photon laser uncaging of glutamate (2PLU) to determine the pre- and postsynaptic actions of mAchRs. Optical quantal analysis revealed that mAchR activation reduces both the probability of glutamate release from the presynaptic terminal and the potency of individual synapses. However, mAchR activation does not directly modulate glutamate receptors. Our results indicate that striatal glutamatergic synapses exhibit a high basal rate of multivesicular release (MVR) without significant saturation of glutamate receptors. We further show that synaptic potency regulates the duration and temporal summation of excitatory postsynaptic potentials. Thus, the combination of basal MVR, lack of receptor saturation, and dendritic nonlinearities allows presynaptic neuromodulation to control both synaptic potency and temporal integration in MSNs.

Results

We measured the effects of mAchR activation on glutamatergic postsynaptic responses in the striatum. In whole-cell current-clamp recordings, paired-pulse electrical stimulation (50 ms interval) evoked depressing excitatory postsynaptic potentials (EPSPs) (Fig.1a). Application of muscarine, a general mAchR agonist, reduced the amplitudes of evoked responses, depolarized the resting membrane potential (V_m) (Fig.1a–c), and increased the paired-pulse ratio (PPR). On average (n=7), muscarine reduced EPSP1 from 8.1±1.6 mV to 4.8±0.8 mV ($p<0.05$) and EPSP2 from 6.5±1.4 mV to 4.9±0.8 mV ($p<0.05$), increasing the PPR from 0.9±0.1 to 1.2±0.1 ($p<0.05$) (Fig.1d). The average V_m depolarized from –73.6±0.8 mV to –67.8±1.6 mV ($p<0.05$, Fig.1d) without significant change in the input resistance (not shown). In whole-cell voltage-clamp recordings (V_{hold}=–75 mV), muscarine reduced the amplitudes of excitatory postsynaptic currents (EPSCs) and increased the PPR (Fig.1e). On average (n=6), muscarine reduced EPSC1 from 131.8±27.5 pA to 86.7±19.3 pA ($p<0.05$) and EPSC2 from 111.7±26.2 pA to 89.9±20.7 pA ($p<0.05$), increasing the PPR

Author Manuscript Author Manuscript Author Manuscript Author Manuscript

from 0.8±0.1 to 1.1±0.1 ($p<0.05$, Fig.1f). These data indicate that mAchR activation exerts both presynaptic (alterations in PPR) and postsynaptic (depolarization) actions in addition to producing effects of unclear origin (reduction of synaptic responses).

Optical quantal analysis of glutamatergic synapses

To determine the effects of mAchR activation at individual synapses, the probability of vesicular release and the synaptic potency (the average response magnitude when release occurs from the presynaptic terminal31, 32) were measured with optical quantal analysis. 2PLSM was used to place a stimulating electrode ~10 μm from spiny regions of proximal dendrite (Fig.2a). Electrode position and stimulus strength were adjusted until a single spine in the field of view was activated, as judged by a Ca-dependent increase in green fluorescence limited to a single spine head (Fig. 2b). Recordings were made in the presence of the AMPAR antagonist NBQX, and the cell was voltage-clamped at 0–10 mV (the empirically determined reversal potential for NMDARs) to eliminate net synaptically-evoked current and prevent changes in potential within the active spine. By collecting evoked fluorescence changes in the spine and neighboring dendrite, success and failure trials could be distinguished (Fig.2c). Under these conditions, synaptic Ca influx occurs through NMDARs and is blocked by the NMDAR antagonist APV (Fig.2d). The probability of success of glutamate release (P_s) was determined as the fraction of trials that evoked a fluorescence transient in the spine head. Synaptic potency (Pot_{NMDA}) was measured as the average amplitude of fluorescence transients in the spine head ($\Delta G/R$) in success trials.

In a separate set of experiments, P_s and Pot_{NMDA} were monitored in individual spines during application of muscarine (Fig.3a). Muscarine increased the fraction of failure trials and decreased $\Delta G/R$ on success trials with no effect on resting fluorescence (Fig.3b). On average (n=10), muscarine decreased P_s from 0.91±0.04 to 0.74±0.05 ($p<0.05$) and Pot_{NMDA} from 34.3±6.1% to 18.4±3.2% ($p<0.05$, Fig.3c).

Uncaging-evoked synaptic currents and Ca transients

To determine if mAchRs directly regulate postsynaptic glutamate receptors, we examined responses evoked by 2-photon laser uncaging of glutamate (2PLU). MSNs were voltage-clamped at –70 mV in the presence of TTX and voltage-gated calcium channel (VGCC) blockers (see methods). To stimulate each spine with a consistent amount of glutamate, laser power was adjusted such that a 500 μs pulse directed at the spine head bleached ~50% of the red fluorescence (Fig.4a–c)33. After setting laser power, the periphery of the spine was probed to find the uncaging position that evoked the largest uncaging-evoked EPSC (uEPSC)34. In the presence of the NMDAR antagonist CPP, uncaging evoked brief inward currents (Fig.4d) with amplitudes similar to those of miniature EPSCs35. On average (n=26), the non-NMDAR-mediated uEPSC was 17.2±1.6 pA (Fig.4e) and was not significantly altered in the presence of muscarine (17.4±2.4 pA, n=24), indicating that mAchR activation does not modulate postsynaptic AMPAR currents.

We performed a similar analysis in the presence of the AMPAR antagonist NBQX and in nominally 0 mM extracellular Mg. In these conditions, at a holding potential of −70 mV, 2PLU evokes NMDAR-mediated uEPSCs and Ca influx into the spine (Fig.5a–d). Neither

Author Manuscript Author Manuscript Author Manuscript Author Manuscript

NMDAR-mediated currents nor Ca influx under control conditions (5.0±0.7 pA and 46.0±6.1% ΔG/R, n=15) were significantly different from those in the presence of muscarine (4.3±0.6 pA and 49.2±6.3% ΔG/R, n=15, Fig.5e). Repeating these experiments under the voltage-clamp conditions used for optical quantal analysis (0–10 mV), there was negligible NMDAR-mediated current flow and muscarine again had no effect on NMDAR-mediated Ca transients (n=19, ΔG/R=195.4±19.2% versus 200.7±27.4% for control and muscarine, respectively, Fig.5f). Thus, although activation of mAchRs regulates NMDAR-mediated synaptic potency, it does not directly modulate the opening probability or Ca permeability of NMDARs.

Presynaptic control of synaptic potency

Our data indicate that mAchR activation alters synaptic potency without any direct modulation of glutamate receptors. Such effects could arise if synapses exhibit MVR and mAchR activation reduces the number of released vesicles. In this case, other manipulations of presynaptic release probability should also alter potency. We therefore examined the effects of the N-type VGCC blocker ω-Conotoxin-GVIA (1.0 μM; Ctx), known to reduce release probability at these synapses15, using optical quantal analysis (Fig.6a). Similar to muscarine application, Ctx increased the fraction of synaptic failures and reduced the amplitude of Ca transients on success trials (Fig.6b). On average (n=5), Ctx application reduced P_s from 0.55±0.12 to 0.30±0.11 (p<0.05) and Pot_{NMDA} from 87.4±8.2% to 57.8±9.2% (p<0.05, Fig.6c). Measurement of 2PLU-evoked Ca transients in neurons clamped at 0–10 mV confirmed a lack of postsynaptic effect of Ctx on NMDAR-mediated Ca transients (Fig.6d).

To further test whether decreased presynaptic release probability could account for the reduction in synaptic potency, we calculated the relative change in Pot_{NMDA} expected for a change in P_s using a Poisson model of vesicular release (see methods). The observed reductions in Pot_{NMDA} for the muscarine and Ctx experiments were well predicted by the decreases in P_s, yielding an average residual error of 19.4% (Fig.6e). In total, our results indicate that direct manipulation of presynaptic release probability alters synaptic potency in the striatum, consistent with a high degree of MVR under basal conditions that is reduced by muscarine or Ctx application.

Glutamate receptors are not saturated in basal conditions

For postsynaptic receptors to follow changes in the concentration of synaptically released glutamate, AMPARs and NMDARs must not be fully saturated. To examine the degree of receptor saturation, we used 2PLU to stimulate spines with different levels of glutamate. Experiments were performed in the presence of TTX and VGCC antagonists, and laser power was set as above (1X condition). Evoked currents were then measured using nominally 0.5X, 1X, and 2X laser power (due to non-uniform intensity during the 500 μs laser pulse, the range of power modulation is less than fourfold). In the presence of NBQX and 0 extracellular Mg (n=13), these three stimuli resulted in NMDAR-mediated uEPSCs of 6.4±1.2 pA, 13.0±2.6 pA, and 21.6±4.1 pA, respectively, and Ca transients of 58.3±10.6%, 90.1±10.6%, and 111.3±10.5%, respectively (Fig.7a). Similar experiments in the presence of CPP (n=11) resulted in non-NMDAR-mediated uEPSCs of 12.5±3.1 pA, 21.1±5.7 pA, and

Author Manuscript Author Manuscript Author Manuscript Author Manuscript

30.3±7.0 pA (Fig.7b). The currents and Ca transients evoked by the 0.5X and 2.0X conditions were significantly different from the 1X-evoked responses (p<0.05, Fig.7cd).

To further study the possibility of receptor saturation, we examined the effect of the low-affinity competitive AMPAR antagonist γ-DGG on electrically-evoked EPSCs. If receptors are significantly saturated by synaptic activation, decreasing glutamate release by reducing extracellular Ca should enhance the current block by γ-DGG. We recorded AMPAR-mediated EPSCs following paired pulse stimulation in the presence of CPP. Application of γ-DGG in control ACSF (2 mM [Ca]) reduced the amplitudes of EPSC1 and EPSC2 and increased PPR (Fig.7e). The increase in PPR is consistent with the relief by γ-DGG of AMPAR desensitization during paired-pulse activation29. On average (n=13), γ-DGG significantly reduced EPSC1 to 35.7±2.9% of control (p<0.05) and increased PPR from 0.77±0.04 to 1.0±0.06 (p<0.05, Fig.7f). Reducing extracellular [Ca] to 1 mM significantly increased PPR (p<0.05, Fig.7f), indicating a reduction in presynaptic release probability. In 1 mM [Ca], on average (n=7), γ-DGG reduced EPSC1 to 43.5±5.6% of control (p<0.05) and increased PPR from 0.97±0.06 to 1.31±0.05 (p<0.05, Fig.7f). The reduction of EPSC amplitude by γ-DGG did not differ between control and low [Ca] conditions, consistent with little AMPAR receptor saturation.

Synaptic potency regulates temporal integration

MSN exhibit voltage-dependent nonlinearities, such as interactions between VGCCs and NMDARs, that enhance the magnitude and summation of synaptic responses29. We theorized that changes in synaptic potency should influence depolarization within active spines and potentially regulate postsynaptic integration. We therefore re-examined modulation of electrically-evoked EPSPs in cells where the somatic V_m was held constant (Fig.8a). At hyperpolarized potentials (Vm=–85 mV), muscarine decreased the EPSP amplitude from 9.5±0.9 mV to 5.0±0.7 mV (n=6, p<0.05) but did not significantly alter the EPSP width (19.2±1.5 ms versus 18.5±0.9 ms for control and muscarine, respectively, Fig. 8b). In cells held at –70 mV, muscarine decreased the average EPSP amplitude from 8.5±0.8 mV to 5.6±1.0 (n=6, p<0.05) and reduced the EPSP width from 32.3±2.3 ms to 25.2±2.5 ms (p<0.05, Fig. 8b). These results suggest that changes in synaptic potency can alter response kinetics by influencing postsynaptic voltage-dependent nonlinearities, although this effect may be absent at hyperpolarized potentials due to mAchR-mediated closure of inwardly rectifying potassium channels28.

To further explore this hypothesis, we mimicked a reduction in synaptic potency by co-applying low concentrations of NBQX and CPP. These agents decrease the strength of activation of individual synapses without confounding alteration of postsynaptic membrane properties. We determined the concentration of NBQX and CPP necessary to reduce AMPAR and NMDAR currents, respectively, by ∼40–50% (the potency decrease seen using optical quantal analysis). In the presence of CPP, application of 0.1 μM NBQX reduced the amplitude of electrically-evoked AMPAR-mediated EPSCs from 158.1±12.2 to 91.8±18.0 pA (n=6). In the presence of NBQX, application of 1.0 μM CPP reduced the amplitude of NMDAR-mediated EPSCs (holding potential=40 mV) from 184.6±22.6 to 106.4±26.9 pA (n=4). These antagonists had no significant effect on the width of either

AMPAR- (3.2±0.2 versus 3.6±0.3 ms) or NMDAR-mediated (83.6±7.3 versus 81.0±6.2 ms) EPSCs (control versus drug, respectively).

We next compared EPSPs evoked in (1) control conditions, (2) following co-application of NBQX (0.1 μM) and CPP (1.0 μM) , and (3) after increasing stimulus strength in the presence of NBQX and CPP to restore the amplitude of the EPSP to that measured control conditions (Fig.8c). This tests the hypothesis that changes in synaptic potency and changes in the total number of active synapses have qualitatively different effects on postsynaptic responses. Co-application of NBQX and CPP reduced the EPSP amplitude and width at half-maximal amplitude (Fig.8c). Increasing stimulus intensity returned the amplitude to that seen in control conditions but did not restore the EPSP width. On average (n=8), decreasing synaptic potency reduced the EPSP amplitude from 11.9±0.9 to 6.6±1.2 mV ($p<0.05$) and the EPSP width from 31.1±4.2 to 22.3±2.8 ms ($p<0.05$, Fig.8d). Increasing the total number of active synapses by increasing stimulus intensity restored the EPSP amplitude (12.4±0.9 mV) but failed to restore the EPSP width (21.9±2.2 ms, $p<0.05$ relative to control), indicating that this parameter is selectively sensitive to the single synapse potency and not to the cumulative multisynaptic depolarization.

The narrowing of the EPSP following reduction in synaptic potency was sufficient to impact temporal summation of synaptic potentials during paired simulation (Fig.8e). On average (n=7), under control conditions, the amplitude of the second EPSP relative to that of the first EPSP at 50 ms and 20 ms intervals was 1.16±0.04 and 1.39±0.08, respectively (Fig.8f). Following co-application of NBQX and CPP and an offsetting increase in stimulation strength, the relative amplitude of the second EPSP was significantly reduced to 0.99±0.04 ($p<0.05$) and 1.12±0.13 ($p<0.05$), respectively. These results demonstrate that modulation of synaptic potency regulates integration independently from changes in the total postsynaptic depolarization.

Discussion

Ach contributes to the regulation of brain function through a diversity of actions[5, 36–38]. Within the striatum, Ach is released by interneurons that receive inputs from the cortex and thalamus, providing feed-forward modulation that is critical for the generation of normal movement and learning in operant conditioning tasks[4, 9–11]. We used optical methods to analyze the pre- and postsynaptic effects of mAchR activation. As described previously, we find that Ach acts presynaptically to reduce the probability of glutamate release at excitatory synapses[15–17, 19]. We also find that striatal glutamatergic synapses exhibit a high basal degree of MVR and that cholinergic reduction of release probability decreases the potency of individual synapses by lowering the concentration of glutamate in the synaptic cleft. Decreasing synaptic potency reduces the duration of postsynaptic EPSPs and limits their temporal summation. Our results provide a detailed description of cholinergic actions at a single central synapse and demonstrate a previously undescribed mechanism of presynaptic control over postsynaptic integration.

Author Manuscript Author Manuscript Author Manuscript Author Manuscript

Author Manuscript Author Manuscript Author Manuscript Author Manuscript

Presynaptic regulation of synaptic potency

Presynaptic terminals of striatal afferent fibers express M2-type mAchRs, whose activation reduces evoked and spontaneous synaptic responses and increases paired pulse ratios (Fig. 1 and 15, 16, 17, 19,23). Thus, mAchR activation decreases release probability, most likely via inhibition of presynaptic P/Q-type VGCCs15 and reduction of action potential-induced Ca increases in the bouton. The postsynaptic actions of mAchR activation are less clear. Previous reports indicate that muscarinic agonists do not alter the response to iontophoretically applied glutamate16 or the amplitude of spontaneous synaptic events23, although one study found that muscarinic agonists enhanced the response to exogenously applied NMDA24. However, activation of postsynaptic M1-type mAchRs inhibits N- and L-type VGCCs as well as multiple potassium conductances25–28, 39, 40, and these effects may indirectly modulate glutamate transmission due to the voltage-dependence of NMDAR opening. Indeed, L-type VGCCs and NMDARs can interact to boost and broaden postsynaptic responses in MSNs29, 30.

Our results show that muscarine reduces synaptic potency by decreasing the concentration of released glutamate in the synaptic cleft. We conclude that the most likely explanation is that striatal glutamatergic boutons release multiple vesicles per action potential under basal conditions. Application of muscarine reduces the probability of release, thereby decreasing the number of fusion events and consequently the synaptic glutamate concentration. This conclusion is dependent on two assumptions. First, that the Ca transient observed in each spine is mediated by glutamate release from a single presynaptic terminal, a position supported by ultrastructural analysis showing that most MSN spines are targeted by a single glutamatergic bouton13, 14. Second, spillover of glutamate from neighboring synapses does not contribute significantly to measured spine Ca transients. In support of this assumption, spine Ca imaging is sensitive to the opening of single NMDARs41, and local electrical stimulation in analyzed experiments did not result in measurable Ca transients in neighboring spines. Additionally, the VGCC blocker ω-conotoxin-GVIA acutely mimicked the actions of muscarine, arguing strongly that changes in glutamate clearance or vesicle filling are unlikely to explain our results.

Multivesicular release has been observed at a variety of central synapses. Cerebellar parallel fiber-Purkinje cell42 and hippocampal CA3-CA1 synapses exhibit low basal release probability31, 43, 44, but MVR can occur when release is enhanced. In contrast, at retinal bipolar cell to amacrine AII ribbon synapses45 and climbing fiber inputs to Purkinje cells46, 47, the probability of release and occurrence of MVR is high under basal conditions. Similarly, we find that striatal glutamatergic synapses have high release probability and a pronounced degree of MVR during basal transmission. The functional consequences of MVR depend on the degree of receptor saturation, which limits the postsynaptic sensitivity to varying glutamate concentration. Using either glutamate uncaging or application of the low-affinity AMPAR antagonist γ-DGG, we find that neither AMPARs nor NMDARs at striatal glutamatergic synapses are saturated despite the occurrence of MVR.

Author Manuscript Author Manuscript Author Manuscript Author Manuscript

Functional consequences

The activity of individual MSNs *in vivo* is dependent on the integration of synchronous synaptic inputs arriving predominantly from the cortex48. Furthermore, integration in MSNs is inherently nonlinear due to engagement of dendritic voltage-dependent conductances and dependence on the spatiotemporal pattern of active synapses29. We found that activation of mAchRs narrowed EPSPs. Moreover, mimicking reduced potency with glutamate receptor antagonists also shortened EPSP duration and decreased temporal summation. This effect was not due to a reduction in the total number of active synapses. One possible explanation is that reduced glutamate per synapse produces less depolarization within individual spines, thus decreasing activation of voltage-sensitive channels including L-type VGCCs and NMDARs29, 30. Our findings differ from previous work showing that mAchR activation increases the duration of EPSPs due to a reduction of an inwardly rectifying potassium conductance28. However, this earlier study was performed at more hyperpolarized potentials and with NMDARs blocked, preventing the voltage-dependent boosting of EPSP amplitude and duration. Indeed, in our experiments, muscarine did not produce a narrowing of EPSPs recorded at −85 mV. Our results suggest that the release of Ach diminishes the ability of MSNs to respond to synchronized cortical inputs, particularly at relatively depolarized potentials seen *in vivo*. Furthermore, they suggest that other striatal modulators of presynaptic release probability, such as endocannabinoids49, are also likely to produce postsynaptic changes in EPSP kinetics and temporal integration. Finally, given the changes in release probability that occur across development, determining the contribution of MVR to synaptic transmission and neuromodulation in older animals remains an interesting avenue of future exploration.

Materials and Methods

Slice preparation and pharmacology

All animal handling was performed in accordance with the Harvard Institutional Animal Care and Use Committee and federal guidelines. Recordings were made from MSNs in striatal slices taken from postnatal day 15–18 Sprague-Dawley rats. Sagittal (Fig. 8) or coronal (Fig. 1–Fig. 7) slices (300 μm thick) were cut in ice-cold external solution containing (in mM): 110 choline, 25 $NaHCO_3$, 1.25 NaH_2PO_4, 2.5 KCl, 7 $MgCl_2$, 0.5 $CaCl_2$, 25 glucose, 11.6 Na-ascorbate, and 3.1 Na-pyruvate, bubbled with 95 % O_2 and 5 % CO_2. Slices were then transferred to artificial cerebrospinal fluid (ACSF) containing (in mM): 127 NaCl, 25 $NaHCO_3$, 1.25 NaH_2PO_4, 2.5 KCl, 1 $MgCl_2$, 2 $CaCl_2$, and 25 glucose, bubbled with 95 % O_2 and 5 % CO_2. After an incubation period of 30–40 min at 34° C, slices were stored at room temperature. All experiments were conducted at 32° C. In all experiments, 10 μM bicuculline, was present in the ACSF to block $GABA_{A/C}$ receptor-mediated inhibition. For all glutamate uncaging experiments, 10 μM serine was included in the ACSF to reduce NMDAR desensitization and VGCCs were blocked with a cocktail of (in μM): 1 ω-conotoxin-MVIIC (N/P/Q-types), 20 nimodipine (L-types), 10 mibefradil (R- and T-types). For some experiments (see text), extracellular $MgCl_2$ was reduced to nominally 0 μM. In experiments in which extracellular Ca was reduced to 1 mM, Mg was increased to 2 mM in order to maintain a constant concentration of divalent ions. Finally, in some experiments (see text), one or more of the following drugs were added to the ACSF,

Author Manuscript Author Manuscript Author Manuscript Author Manuscript

unless otherwise stated, at the following concentrations (in μM): 10 muscarine, 10 NBQX, 10 CPP, 50 APV, 1 TTX, 1 ω-conotoxin-GVIA, 2500 γ-DGG. In order to block ~50% of AMPARs and NMDARs (Fig. 8), 0.1 and 1 μM of NBQX and CPP were used, respectively. All chemicals were from Sigma or Tocris, with the exception of ω-conotoxin-GVIA and ω-conotoxin-MVIIC (Peptides International, Inc.).

Electrophysiology and imaging

Whole-cell recordings were obtained from MSNs identified with video-IR/DIC and 2-photon laser scanning microscopy (2PLSM) based on their small cell bodies and prominent dendritic spines. For current clamp recordings, glass electrodes (2–4 MΩ) were filled with internal solution containing (in mM): 135 $KMeSO_3$, 10 HEPES, 4 $MgCl_2$, 4 Na_2ATP, 0.4 NaGTP, and 10 $Na_2CreatinePO_4$, adjusted to pH 7.4 with KOH. For voltage clamp recordings, cesium was substituted for potassium to improve space clamping. For physiology-only experiments, 1 mM EGTA and 20 μM Alexa Fluor-594 (to image neuronal morphology) were added to the internal solution. For Ca imaging experiments, 300 μM of the Ca sensitive indicator Fluo-5F and 20 μM Alexa Fluor-594 were added. Current and voltage recordings were made using a Multiclamp 700B amplifier. Data was filtered at 5 kHz and digitized at 10 kHz. Excitatory input fibers were stimulated with a small glass electrode (tip diameter 2 – 4 μm) filled with ACSF using brief (0.2 ms) current injections. For paired-pulse stimulation experiments, the electrode was placed at the border between the striatum and the overlying white matter. For optical quantal analysis experiments, the electrode was placed ~10 μm from the dendritic spine of interest.

Intracellular Ca imaging and glutamate uncaging were accomplished with a custom microscope combining 2PLSM and 2PLU, as previously described33, 35. Neurons were filled via the patch electrode for 10–15 minutes before imaging. Fluo-5F (green) and Alexa Fluor-594 (red) were excited using 840 nm light to monitor Ca signals and spine morphology, respectively. To measure Ca signals, green and red fluorescence were collected during 500 Hz line scans across a spine and a neighboring dendrite. Ca signals were quantified as increases in green fluorescence from baseline normalized to the red fluorescence (ΔG/R). Reference frame scans were taken between each acquisition in order to correct for small spatial drift of the preparation over time.

For 2PLU experiments, MNI-glutamate was bath applied at 2.5 mM, and glutamate uncaging was achieved using a 0.5 ms pulse of 720 nm light. In order to achieve standard uncaging power, (which translates into a constant amount of glutamate uncaged on each trial) we used photobleaching of Alexa Fluo-594 in the spine of interest as previously described33. Bleaching is a function of the laser power and thus provides readout of power delivery that is independent of spine depth and electrophysiological responses.

Data acquisition and analysis

Imaging and physiology data were acquired using National Instruments boards and custom software written in MATLAB (Mathworks)50. Off-line analysis was performed using custom routines written in MATLAB and Igor Pro (Wavemetrics). Peak amplitudes of electrically evoked EPSPs were calculated by averaging a 3 ms window around the peak.

Author Manuscript Author Manuscript Author Manuscript Author Manuscript

The amplitudes of electrically evoked EPSCs and uncaging-evoked EPSCs mediated by AMPARs were calculated by averaging over a 2 ms window, whereas a 10 ms window was used to calculate peaks of NMDAR-mediated EPSCs. EPSP and EPSC widths were calculated as the interval between points at half-maximal amplitude. For imaging experiments, measurements of ΔG/R were calculated by taking the average of the signal over a 150 ms post-stimulus window. For paired-pulse experiments, we measured the response to a single stimulation or paired stimulation at an interstimulus interval of 50 or 20 ms. The paired-pulse ratio (PPR) was calculated by subtracting the response to the single stimulus from that to the paired stimulus and then calculating the ratio of the peak of the remaining response to the single response.

For optical quantal analysis, successes were distinguished from failures by setting a threshold equal to two standard deviations above baseline noise. To determine the effect of muscarine and conotoxin-GVIA on the amplitude of NMDAR-mediated Ca signals, the average ΔG/R on success trials during the baseline period were compared to the average ΔG/R after application of each drug. The probability of success was calculated by dividing the number of success trials by the total number of trials during either baseline or after bath application of each drug. To ensure that the dendrite was not stimulated directly, analysis was limited to those experiments in which Ca entry was confined to a single spine.

In sections describing optical or uncaging responses measured from individual spines, the stated n indicates the number of spines analyzed. In sections describing electrically-evoked synaptic responses, the stated n indicates the number of cells analyzed. All statistics are expressed as mean±SEM and comparisons were made using a two-tailed Student's t-test. Differences were judged statistically significant for $p<0.05$.

Poisson Model

In order to test whether reduced probability of vesicle release could adequately explain the observed changes in postsynaptic potency, we developed a Poisson model of synaptic transmission that assumes independent release of multiple docked vesicles per active zone. In this model, the probability of release of 'x' vesicles following an action potential is given by a function of a single parameter 'λ' that is the average number of released vesicles (i.e., $\lambda = \langle x \rangle$), such that:

$$P(x)=\frac{\lambda^x e^{-\lambda}}{x!}$$

Therefore, the probability of release of one or more vesicles (i.e., P_s, the probability of seeing a synaptic response on any given trial) is related to λ by:

$$\lambda = -\ln(\mathrm{P}(0)) = -\ln(1-\mathrm{P_s}).$$

Assuming a linear relationship between the number of released vesicles and the degree of NMDAR activation, the mean spine head Ca transient amplitude (averaged across all trials including successes and failures) is given by:

Author Manuscript Author Manuscript Author Manuscript Author Manuscript

$$<\Delta G/R>=\lambda q$$

where q is the quantal postsynaptic amplitude for a single vesicle. Furthermore, the mean spine head Ca transient amplitude of only success trials (the synaptic potency, Pot_{NMDA}) is:

$$Pot_{NMDA}=\lambda q/P_s=-\ln(1-P_s)q/P_s.$$

If the quantal amplitude q is the same in two conditions (i.e., before and after drug application), the ratio of synaptic potencies in the two conditions is purely a function of the probability of successful vesicular release:

$$Pot_1/Pot_2=[\ln(1-P_{s1})/P_{s1}]/[\ln(1-P_{s2})/P_{s2}] \quad \text{(eq. 1)}$$

(eq. 1) Figure 6e shows the results of using this equation to predict changes in synaptic potency for all experiments involving either muscarine or conotoxin-GVIA application. We plotted the expected fractional change in Pot_{NMDA} as a function of the observed change in P_s. The model ignores possible supralinearities in the activation of NMDARs due to a Hill coefficient of greater than 1 for activation by glutamate and possible sublinearities due to saturation of Ca indicator. Despite these simplifications and the lack of free parameters, eq. 1 fits the experimental data with a residual error of <20%.

Acknowledgements

The authors thank members of the Sabatini lab, Adam Carter, Wade Regehr, and Jessica Cardin for helpful comments during the preparation of this manuscript. This work was funded by a Parkinson’s Disease Foundation Postdoctoral Fellowship (MJH); a Quan Predoctoral Fellowship and NINDS predoctoral NRSA (1 F31 NS049655-01) (GSL); and a grant from NINDS (NS046579) (BLS).

REFERENCES

1. Shepherd, GM. The Synaptic Organization of the Brain. Oxford: Oxford University Press; 2004.
2. Berton O, Nestler EJ. New approaches to antidepressant drug discovery: beyond monoamines. Nat Rev Neurosci. 2006; 7:137–151. [PubMed: 16429123]
3. Iversen SD, Iversen LL. Dopamine: 50 years in perspective. Trends Neurosci. 2007; 30:188–193. [PubMed: 17368565]
4. Pisani A, Bernardi G, Ding J, Surmeier DJ. Re-emergence of striatal cholinergic interneurons in movement disorders. Trends Neurosci. 2007; 30:545–553. [PubMed: 17904652]
5. Lucas-Meunier E, Fossier P, Baux G, Amar M. Cholinergic modulation of the cortical neuronal network. Pflugers Arch. 2003; 446:17–29. [PubMed: 12690458]
6. Bolam JP, Hanley JJ, Booth PA, Bevan MD. Synaptic organisation of the basal ganglia. J Anat. 2000; 196(Pt 4):527–542. [PubMed: 10923985]
7. DeLong MR. Primate models of movement disorders of basal ganglia origin. Trends Neurosci. 1990; 13:281–285. [PubMed: 1695404]
8. Graybiel AM. The basal ganglia. Curr Biol. 2000; 10:R509–R511. [PubMed: 10899013]
9. Kaneko S, et al. Synaptic integration mediated by striatal cholinergic interneurons in basal ganglia function. Science. 2000; 289:633–637. [PubMed: 10915629]
10. Kitabatake Y, Hikida T, Watanabe D, Pastan I, Nakanishi S. Impairment of reward-related learning by cholinergic cell ablation in the striatum. Proc Natl Acad Sci U S A. 2003; 100:7965–7970. [PubMed: 12802017]

Author Manuscript Author Manuscript Author Manuscript Author Manuscript

11. Apicella P. Leading tonically active neurons of the striatum from reward detection to context recognition. Trends Neurosci. 2007; 30:299–306. [PubMed: 17420057]
12. Calabresi P, Centonze D, Gubellini P, Pisani A, Bernardi G. Acetylcholine-mediated modulation of striatal function. Trends Neurosci. 2000; 23:120–126. [PubMed: 10675916]
13. Kemp JM, Powell TP. The termination of fibres from the cerebral cortex and thalamus upon dendritic spines in the caudate nucleus: a study with the Golgi method. Philos Trans R Soc Lond B Biol Sci. 1971; 262:429–439. [PubMed: 4107496]
14. Wilson CJ, Groves PM. Fine structure and synaptic connections of the common spiny neuron of the rat neostriatum: a study employing intracellular inject of horseradish peroxidase. J Comp Neurol. 1980; 194:599–615. [PubMed: 7451684]
15. Barral J, Galarraga E, Bargas J. Muscarinic presynaptic inhibition of neostriatal glutamatergic afferents is mediated by Q-type Ca2+ channels. Brain Res Bull. 1999; 49:285–289. [PubMed: 10424849]
16. Malenka RC, Kocsis JD. Presynaptic actions of carbachol and adenosine on corticostriatal synaptic transmission studied in vitro. J Neurosci. 1988; 8:3750–3756. [PubMed: 2848109]
17. Pakhotin P, Bracci E. Cholinergic interneurons control the excitatory input to the striatum. J Neurosci. 2007; 27:391–400. [PubMed: 17215400]
18. Calabresi P, Centonze D, Gubellini P, Pisani A, Bernardi G. Blockade of M2-like muscarinic receptors enhances long-term potentiation at corticostriatal synapses. Eur J Neurosci. 1998; 10:3020–3023. [PubMed: 9758172]
19. Sugita S, Uchimura N, Jiang ZG, North RA. Distinct muscarinic receptors inhibit release of gamma-aminobutyric acid and excitatory amino acids in mammalian brain. Proc Natl Acad Sci U S A. 1991; 88:2608–2611. [PubMed: 1672454]
20. Aznavour N, Mechawar N, Watkins KC, Descarries L. Fine structural features of the acetylcholine innervation in the developing neostriatum of rat. J Comp Neurol. 2003; 460:280–291. [PubMed: 12687691]
21. Izzo PN, Bolam JP. Cholinergic synaptic input to different parts of spiny striatonigral neurons in the rat. J Comp Neurol. 1988; 269:219–234. [PubMed: 3281983]
22. Galarraga E, et al. Cholinergic modulation of neostriatal output: a functional antagonism between different types of muscarinic receptors. J Neurosci. 1999; 19:3629–3638. [PubMed: 10212321]
23. Hernandez-Echeagaray E, Galarraga E, Bargas J. 3-Alpha-chloro-imperialine, a potent blocker of cholinergic presynaptic modulation of glutamatergic afferents in the rat neostriatum. Neuropharmacology. 1998; 37:1493–1502. [PubMed: 9886672]
24. Calabresi P, Centonze D, Gubellini P, Pisani A, Bernardi G. Endogenous ACh enhances striatal NMDA-responses via M1-like muscarinic receptors and PKC activation. Eur J Neurosci. 1998; 10:2887–2895. [PubMed: 9758158]
25. Howe AR, Surmeier DJ. Muscarinic receptors modulate N-, P-, and L-type Ca2+ currents in rat striatal neurons through parallel pathways. J Neurosci. 1995; 15:458–469. [PubMed: 7823150]
26. Perez-Rosello T, et al. Cholinergic control of firing pattern and neurotransmission in rat neostriatal projection neurons: role of CaV2.1 and CaV2.2 Ca2+ channels. J Neurophysiol. 2005; 93:2507–2519. [PubMed: 15615835]
27. Shen W, Hamilton SE, Nathanson NM, Surmeier DJ. Cholinergic suppression of KCNQ channel currents enhances excitability of striatal medium spiny neurons. J Neurosci. 2005; 25:7449–7458. [PubMed: 16093396]
28. Shen W, et al. Cholinergic modulation of Kir2 channels selectively elevates dendritic excitability in striatopallidal neurons. Nat Neurosci. 2007; 10:1458–1466. [PubMed: 17906621]
29. Carter AG, Soler-Llavina GJ, Sabatini BL. Timing and location of synaptic inputs determine modes of subthreshold integration in striatal medium spiny neurons. J Neurosci. 2007; 27:8967–8977. [PubMed: 17699678]
30. Liu JC, et al. Calcium modulates dopamine potentiation of N-methyl-D-aspartate responses: electrophysiological and imaging evidence. J Neurosci Res. 2004; 76:315–322. [PubMed: 15079860]
31. Oertner TG, Sabatini, Nimchinsky, Svoboda. Facilitation at single synapses probed with optical quantal analysis. Nat Neurosci. 2002; 5:657–664. [PubMed: 12055631]

32. Stevens CF, Wang Y. Facilitation and depression at single central synapses. Neuron. 1995; 14:795–802. [PubMed: 7718241]
33. Bloodgood BL, Sabatini BL. Nonlinear regulation of unitary synaptic signals by CaV(2.3) voltage-sensitive calcium channels located in dendritic spines. Neuron. 2007; 53:249–260. [PubMed: 17224406]
34. Busetto G, Higley MJ, Sabatini BL. Developmental presence and disappearance of postsynaptically silent synapses on dendritic spines of rat layer 2/3 pyramidal neurons. J Physiol. 2008; 586:1519–1527. [PubMed: 18202095]
35. Carter AG, Sabatini BL. State-dependent calcium signaling in dendritic spines of striatal medium spiny neurons. Neuron. 2004; 44:483–493. [PubMed: 15504328]
36. Hasselmo ME. The role of acetylcholine in learning and memory. Curr Opin Neurobiol. 2006; 16:710–715. [PubMed: 17011181]
37. Jones BE. Activity, modulation and role of basal forebrain cholinergic neurons innervating the cerebral cortex. Prog Brain Res. 2004; 145:157–169. [PubMed: 14650914]
38. McCormick DA. Actions of acetylcholine in the cerebral cortex and thalamus and implications for function. Prog Brain Res. 1993; 98:303–308. [PubMed: 8248519]
39. Akins PT, Surmeier DJ, Kitai ST. Muscarinic modulation of a transient K+ conductance in rat neostriatal neurons. Nature. 1990; 344:240–242. [PubMed: 2314459]
40. Olson PA, et al. G-protein-coupled receptor modulation of striatal CaV1.3 L-type Ca2+ channels is dependent on a Shank-binding domain. J Neurosci. 2005; 25:1050–1062. [PubMed: 15689540]
41. Nimchinsky EA, Yasuda R, Oertner TG, Svoboda K. The number of glutamate receptors opened by synaptic stimulation in single hippocampal spines. J Neurosci. 2004; 24:2054–2064. [PubMed: 14985448]
42. Foster KA, Crowley JJ, Regehr. The influence of multivesicular release and postsynaptic receptor saturation on transmission at granule cell to Purkinje cell synapses. J Neurosci. 2005; 25:11655–11665. [PubMed: 16354924]
43. Christie JM, Jahr CE. Multivesicular release at Schaffer collateral-CA1 hippocampal synapses. J Neurosci. 2006; 26:210–216. [PubMed: 16399689]
44. Tong, Jahr CE. Multivesicular release from excitatory synapses of cultured hippocampal neurons. Neuron. 1994; 12:51–59. [PubMed: 7507341]
45. Singer JH, Lassova L, Vardi N, Diamond JS. Coordinated multivesicular release at a mammalian ribbon synapse. Nat Neurosci. 2004; 7:826–833. [PubMed: 15235608]
46. Foster KA, Kreitzer AC, Regehr. Interaction of postsynaptic receptor saturation with presynaptic mechanisms produces a reliable synapse. Neuron. 2002; 36:1115–1126. [PubMed: 12495626]
47. Wadiche JI, Jahr CE. Multivesicular release at climbing fiber-Purkinje cell synapses. Neuron. 2001; 32:301–313. [PubMed: 11683999]
48. Wilson CJ, Kawaguchi Y. The origins of two-state spontaneous membrane potential fluctuations of neostriatal spiny neurons. J Neurosci. 1996; 16:2397–2410. [PubMed: 8601819]
49. Adermark L, Lovinger DM. Frequency-dependent inversion of net striatal output by endocannabinoid-dependent plasticity at different synaptic inputs. J Neurosci. 2009; 29:1375–1380. [PubMed: 19193884]
50. Pologruto TA, Sabatini BL, Svoboda K. ScanImage: flexible software for operating laser scanning microscopes. Biomed Eng Online. 2003; 2:13. [PubMed: 12801419]

Author Manuscript Author Manuscript Author Manuscript Author Manuscript

Author Manuscript Author Manuscript Author Manuscript Author Manuscript

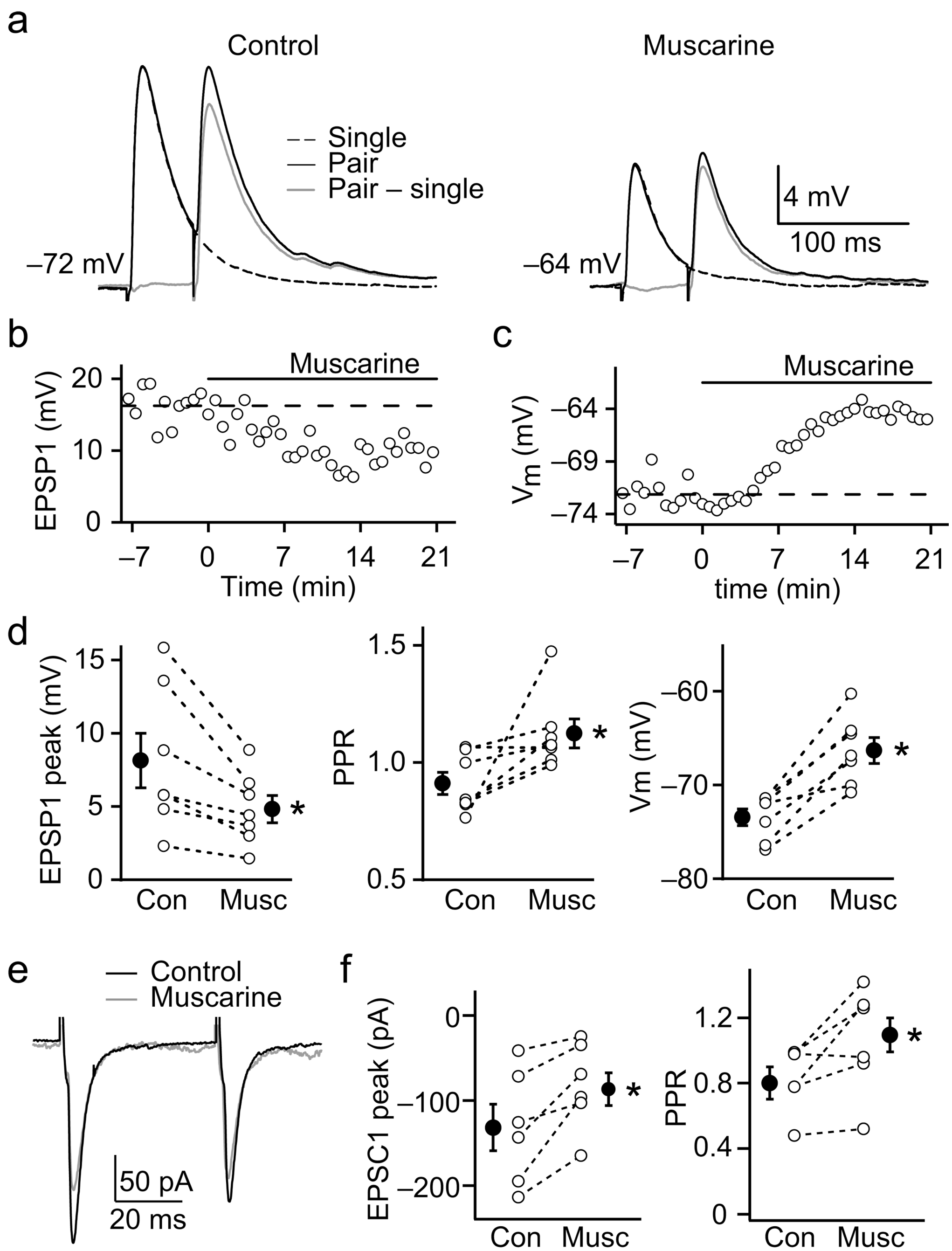

Figure 1. Modulation of synaptic responses and passive properties of MSNs by mAchRs

(a) *left*, Single (dashed line) and paired (solid, black line) EPSPs recorded from a MSN in control conditions. The difference between the paired and single EPSP is shown (gray). *right*, EPSPs recorded after wash-in of 10 μM muscarine. EPSPs are averages of 10 consecutive trials.

(b) Time course of the first EPSP (EPSP1) amplitude from the experiment shown in (a). Muscarine was applied during the time indicated by the horizontal bar.

(c) Time course of the resting membrane potential (V_m) from the experiment shown in (a).

Author Manuscript
Author Manuscript
Author Manuscript
Author Manuscript

(d) EPSP1 peak amplitude (*left*), PPR (*middle*), and V_m (*right*) for each recorded cell (open circles) in control conditions (con) and after muscarine wash-in (musc). Mean values±SEM are shown (closed circles).

(e) Paired EPSCs recorded from a MSN under voltage clamp (holding potential was –75 mV) before (black sold line) and after (gray solid line) application of muscarine.

(f) EPSC1 peak amplitude (*left*) and PPR (*right*) for each recorded cell (open circles) before and after muscarine wash-in. Mean values±SEM are shown (closed circles).

* indicates a significant difference between groups ($p<0.05$).

Author Manuscript Author Manuscript Author Manuscript Author Manuscript

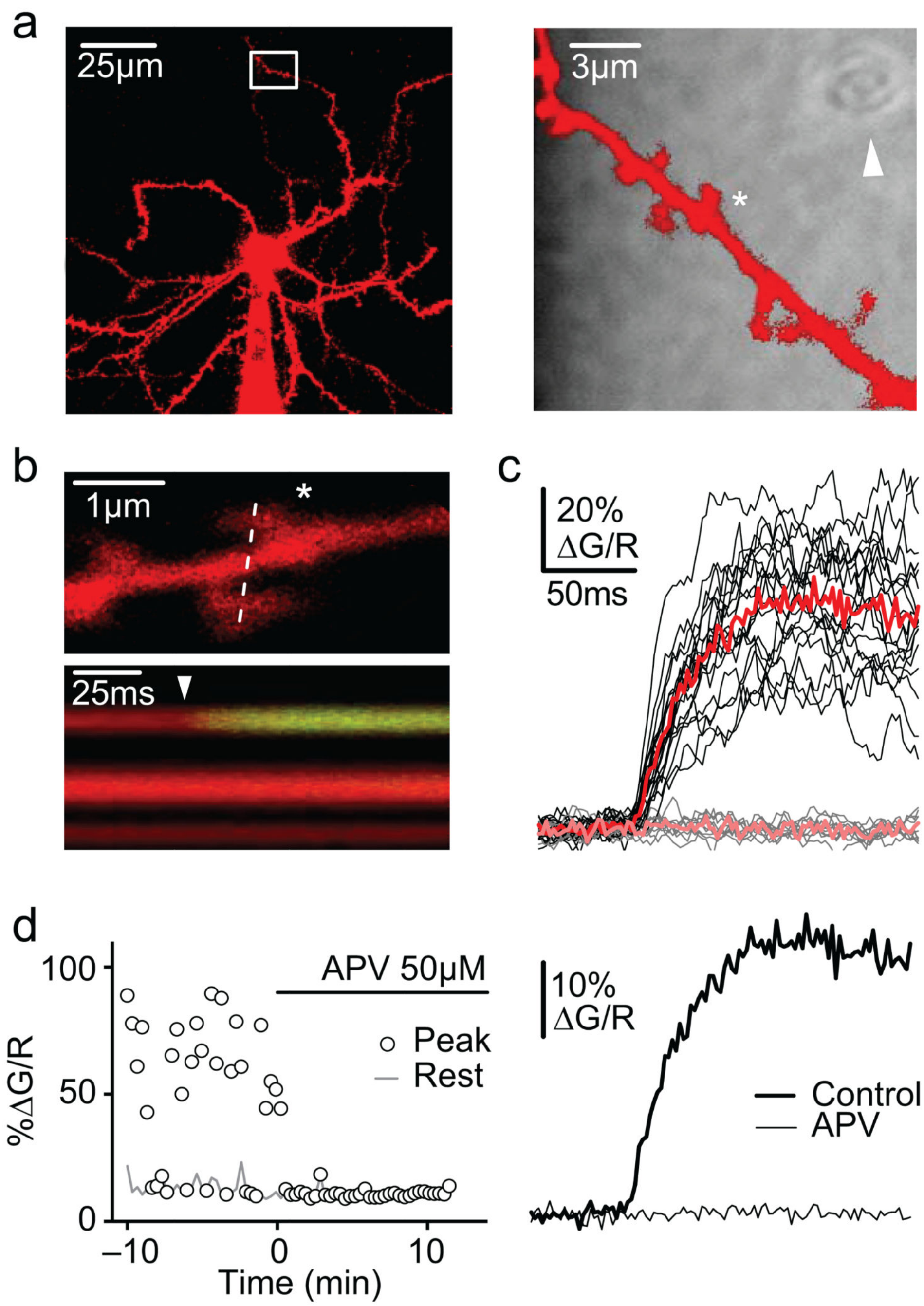

Figure 2. Optical quantal analysis of synaptic potency and failure rate

(a) *left*, 2PLSM image of an MSN filled with 20 μM Alexa-594 and 300 μM Fluo-5F. *right*, Higher magnification image of indicated region. The segment of dendrite is shown overlaid on a laser-scanning differential interference contrast image of the slice. The extracellular stimulating electrode (arrowhead) is located near a spine containing an activated synapse (*).

(b) *top*, Enlarged image of the dendrite shown in (a). *bottom*, Fluorescence collected in a line scan as indicated by the dashed line in the top panel during electrically-evoked synaptic activation. The image is an average of 19 success trials. The stimulus evokes a Ca transient that is limited to the upper (*) spine.

(c) Quantification of synaptically evoked fluorescence transients (ΔG/R) in the active spine showing successes (black) and failures (gray) of synaptic transmission. The red and pink traces are the averages of the black and gray traces, respectively.

(d) *left*, Time course of the peak ΔG/R (circles) and resting fluorescence (gray line) during a 10 minute baseline period and after application of the NMDAR antagonist APV (50 μM). The baseline period of this time course corresponds to the traces shown in (c). *right*, Average of 30 consecutive trials (successes and failures) during the baseline (thick line) and in the presence of APV (thin line).

Author Manuscript Author Manuscript Author Manuscript Author Manuscript

Author Manuscript Author Manuscript Author Manuscript Author Manuscript

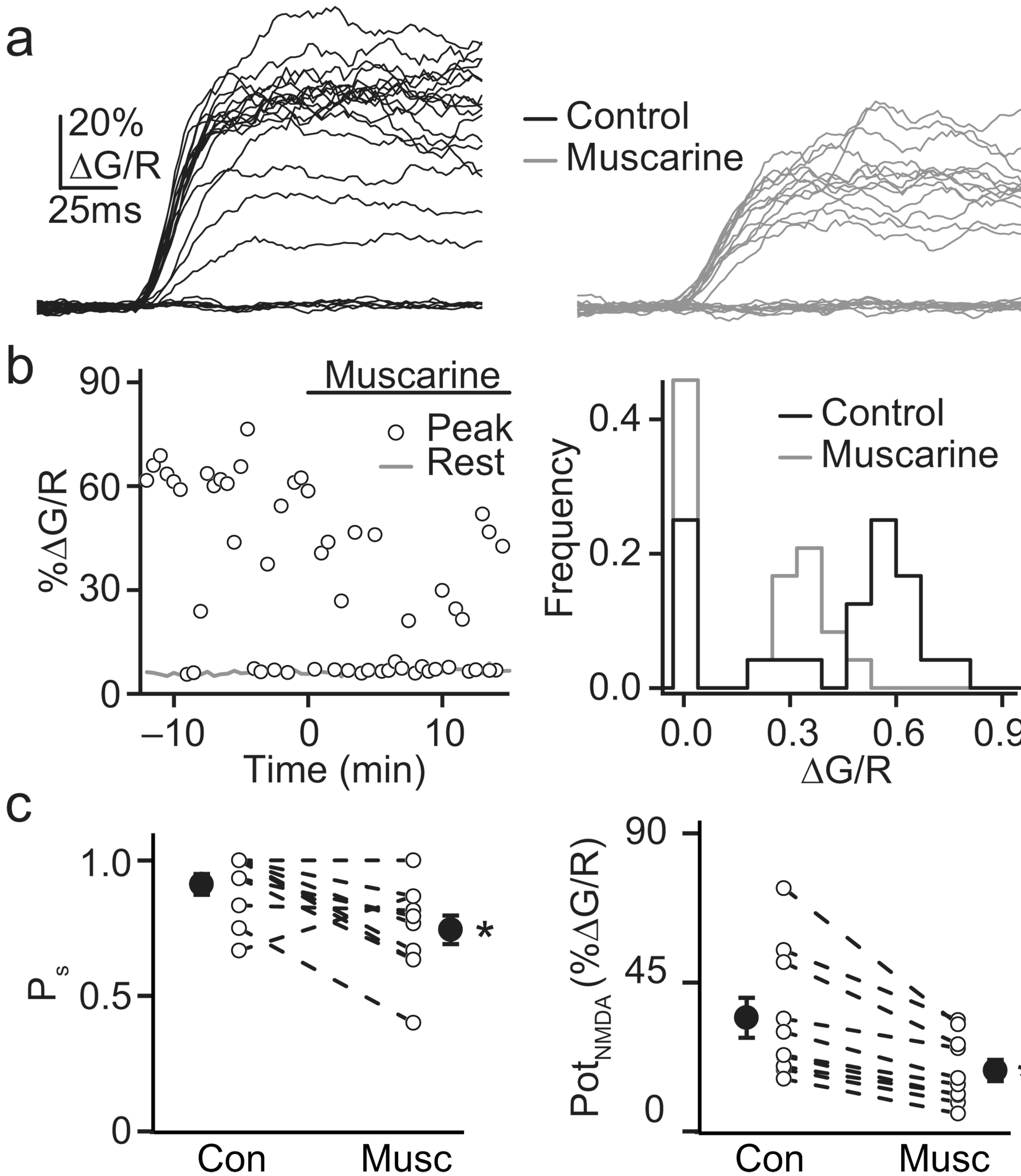

Figure 3. mAchR activation increases synaptic failures and decreases NMDAR-mediated synaptic potency

(a) *left*, ΔG/R from a representative spine in control ACSF showing synaptic successes and failures. *right*, ΔG/R in the same spine after bath application of muscarine (10 μM).

(b) *left*, Time course of the peak ΔG/R (circles) and resting fluorescence (gray line) during a baseline period and after application of muscarine. *right*, Corresponding histogram of ΔG/R amplitudes in the two conditions.

(c) Probability of success (P_s) (*left*) and synaptic potency (Pot_{NMDA}) (*right*) for each spine (open circles) under control conditions (Con) and after wash-in of muscarine (Musc). Mean values±SEM are shown (closed circles).

* indicates a significant difference between groups ($p<0.05$).

Author Manuscript

Author Manuscript

Author Manuscript

Author Manuscript

Author Manuscript
Author Manuscript
Author Manuscript
Author Manuscript

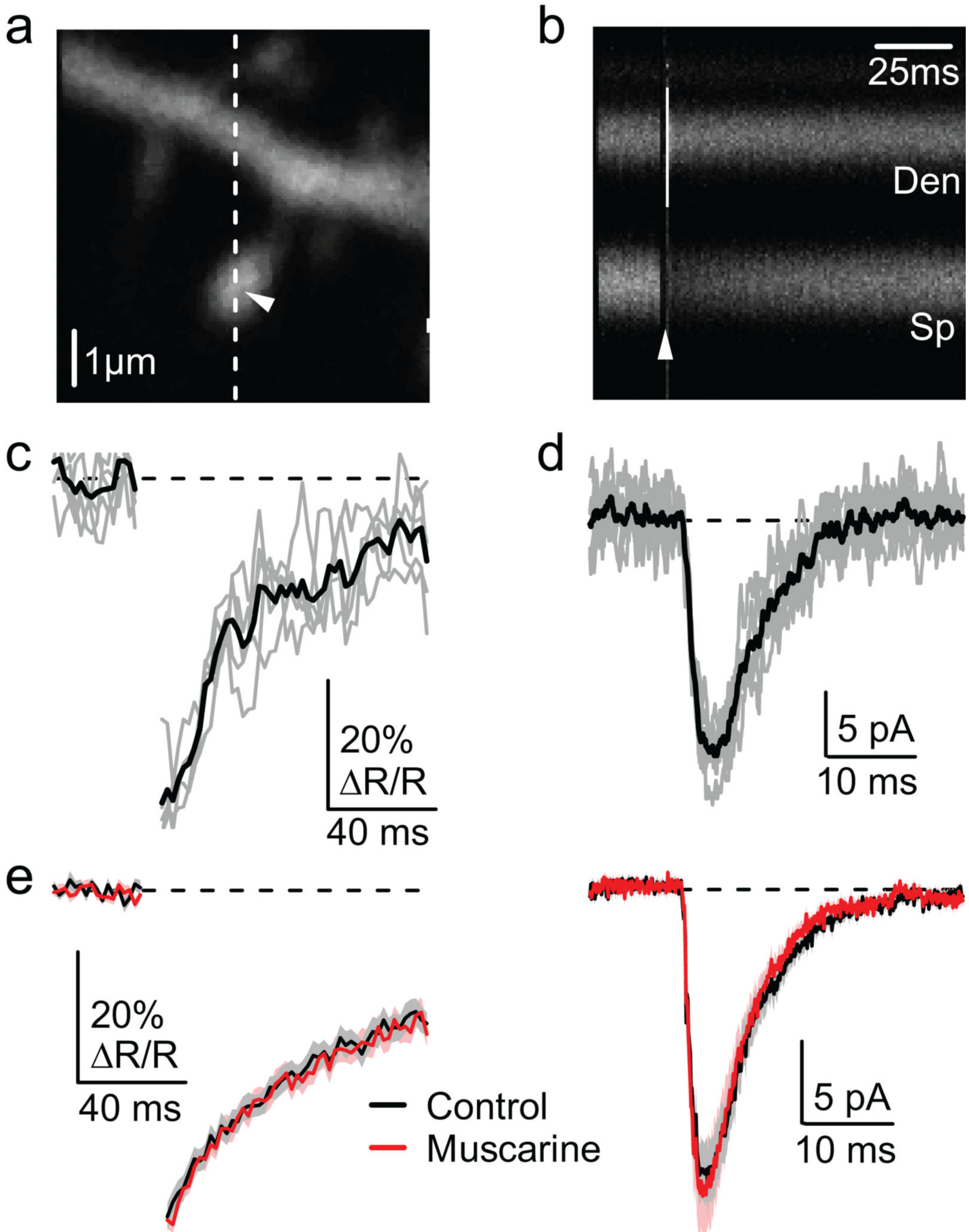

Figure 4. Activation of mAchRs does not modulate AMPAR-mediated currents

(a) 2PLSM image of a spiny region from an MSN dendrite filled with 20 µM Alexa-594.

(b) Red fluorescence in the spine head (Sp) and neighboring dendrite (Den) measured in line scan over the region indicated in (a). The arrowheads in (a) and (b) indicate the location and timing, respectively, of a 500 µs pulse of 720 laser light used to photobleach Alexa-594 fluorescence in the spine head.

(c) Five consecutive red fluorescence bleaching (~50%) trials (gray) and the corresponding average (black) used to standardize laser power.

(d) AMPAR-mediated uEPSC evoked by 2PLU of MNI-glutamate in the presence of the NMDAR antagonist CPP (10 μM) using the laser power determined in (c). Individual trials (gray traces) and the corresponding average (black trace) are shown.

(e) Average photobleaching transients (*left*) and AMPAR mediated uEPSCs (*right*) measured in control conditions (black, n=26 spines) and in the presence of muscarine (red, n=25 spines). Solid lines indicate the mean and the shaded regions indicate the mean±SEM.

Author Manuscript
Author Manuscript
Author Manuscript
Author Manuscript

Author Manuscript Author Manuscript Author Manuscript Author Manuscript

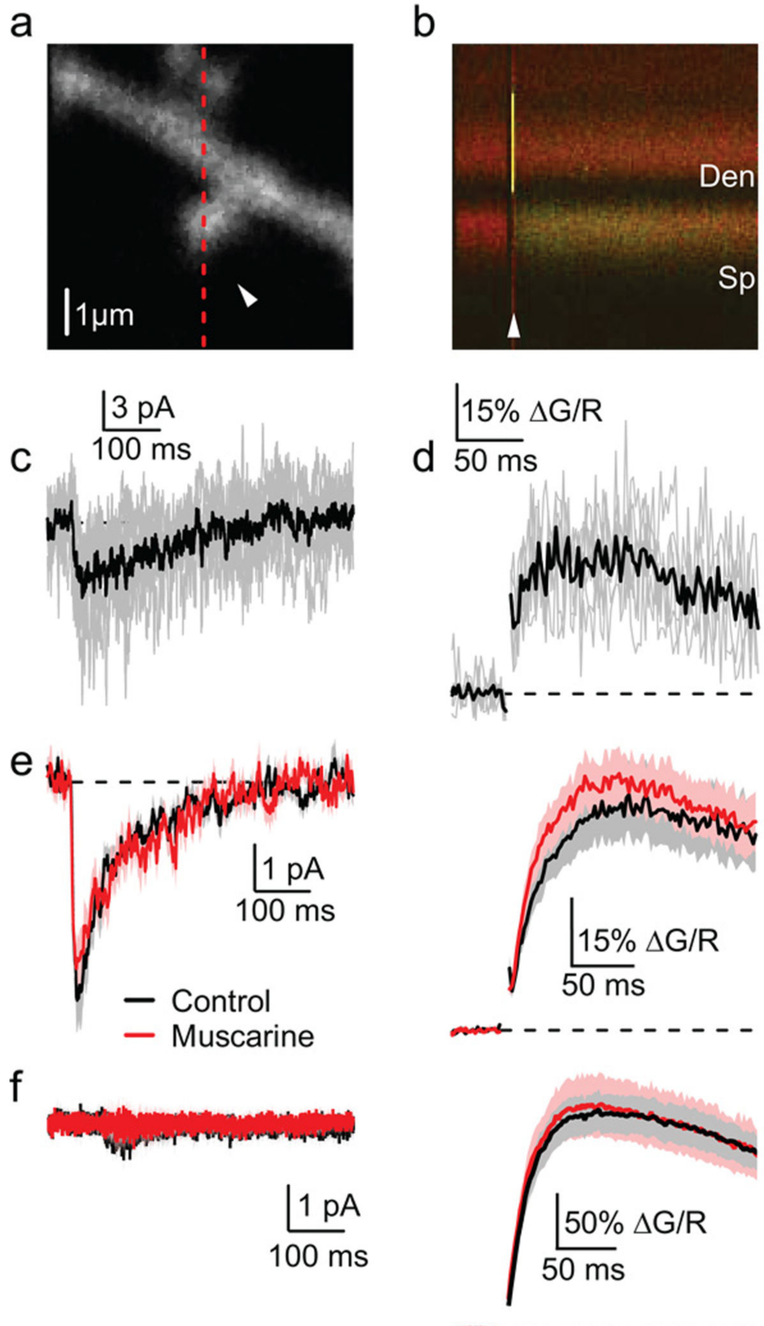

Figure 5. Activation of mAchRs does not modulate NMDAR-mediated currents or Ca transients

(a) 2PLSM image of a spiny region from an MSN dendrite filled with 20 μM Alexa-594 and 300 μM Fluo-5F.

(b) Red and green fluorescence in the spine head (Sp) and neighboring dendrite (Den) measured in line scan over the region indicated by the dashed line from (a). The arrowheads in (a) and (b) indicate the location and timing, respectively, of a 500 μs pulse of 720 nm laser light. The increase in green fluorescence indicates increased intracellular Ca. Power was calibrated as in Figure 4.

Author Manuscript

(c) NMDAR-mediated uEPSC evoked by glutamate uncaging in the presence of nominally 0 extracellular Mg and the AMPAR antagonist NBQX (10 μM). Individual trials (gray traces) and the corresponding average (black trace) are shown.

(d) NMDAR-mediated Ca transients recorded simultaneously with uEPSCs shown in (c).

(e) Average (lines) and average±SEM (shaded region) of NMDAR-mediated uEPSCs (*left*) and spine head Ca transients (*right*) in control conditions (black, n=21 spines) and in the presence of muscarine (red, n=13 spines).

(f) As in (e) for data collected in the same conditions used for optical quantal analysis. Each cell was held at the reversal potential for NMDAR-mediated current (∼ 0–10 mV) and in the presence of 1 mM extracellular Mg.

Author Manuscript
Author Manuscript
Author Manuscript
Author Manuscript

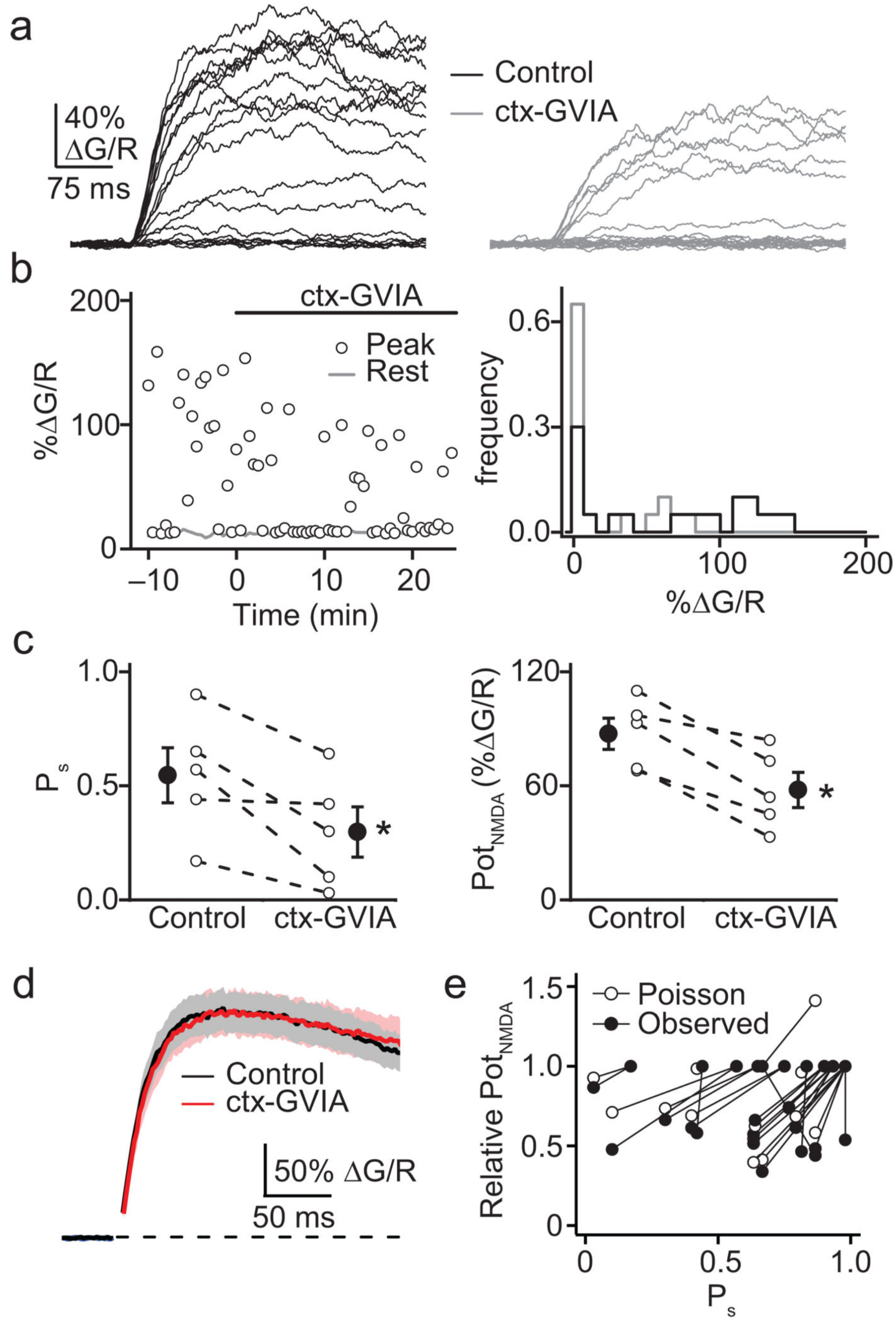

Figure 6. Direct inhibition of vesicular release by blockade of presynaptic N-type Ca channels reduces synaptic potency

(a) ΔG/R measured from a single active spine as in Figure 3 in control conditions (*left*) and after bath application of ω-conotoxin-GVIA (1 μM) (*right*).

(b) *left*, Time course of the peak ΔG/R (circles) and resting fluorescence (gray line) during a baseline period and after application of ω-conotoxin-GVIA. *right*, Corresponding histogram of ΔG/R amplitudes in the two conditions.

(c) Probability of success (P_s) (*left*) and synaptic potency (Pot_{NMDA}) (*right*) for each spine (open circles) under control conditions (Con) and after wash-in of ω-conotoxin-GVIA (ctx-GVIA). Mean values±SEM are shown (closed circles).

(d) Average (lines) and average±SEM (shaded region) of NMDAR-mediated spine head Ca transients evoked by glutamate uncaging in control conditions (black, n=21 spines) and in the presence of ω-conotoxin-GVIA (red, n=13 spines). Each cell was voltage-clamped at 0–10 mV in the presence of 1 mM extracellular Mg.

(e) Relative synaptic potency (Pot_{NMDA}) before and after muscarine or ω-conotoxin-GVIA application plotted against the corresponding probability of success (P_s). Lines connect values from the same synapse. Closed circles depict the experimental data. Open circles depict the relative potency expected for the observed changes in P_s in a Poisson model of synaptic release (see Methods).

* indicates a significant difference between groups ($p<0.05$).

Author Manuscript Author Manuscript Author Manuscript Author Manuscript

Author Manuscript
Author Manuscript
Author Manuscript
Author Manuscript

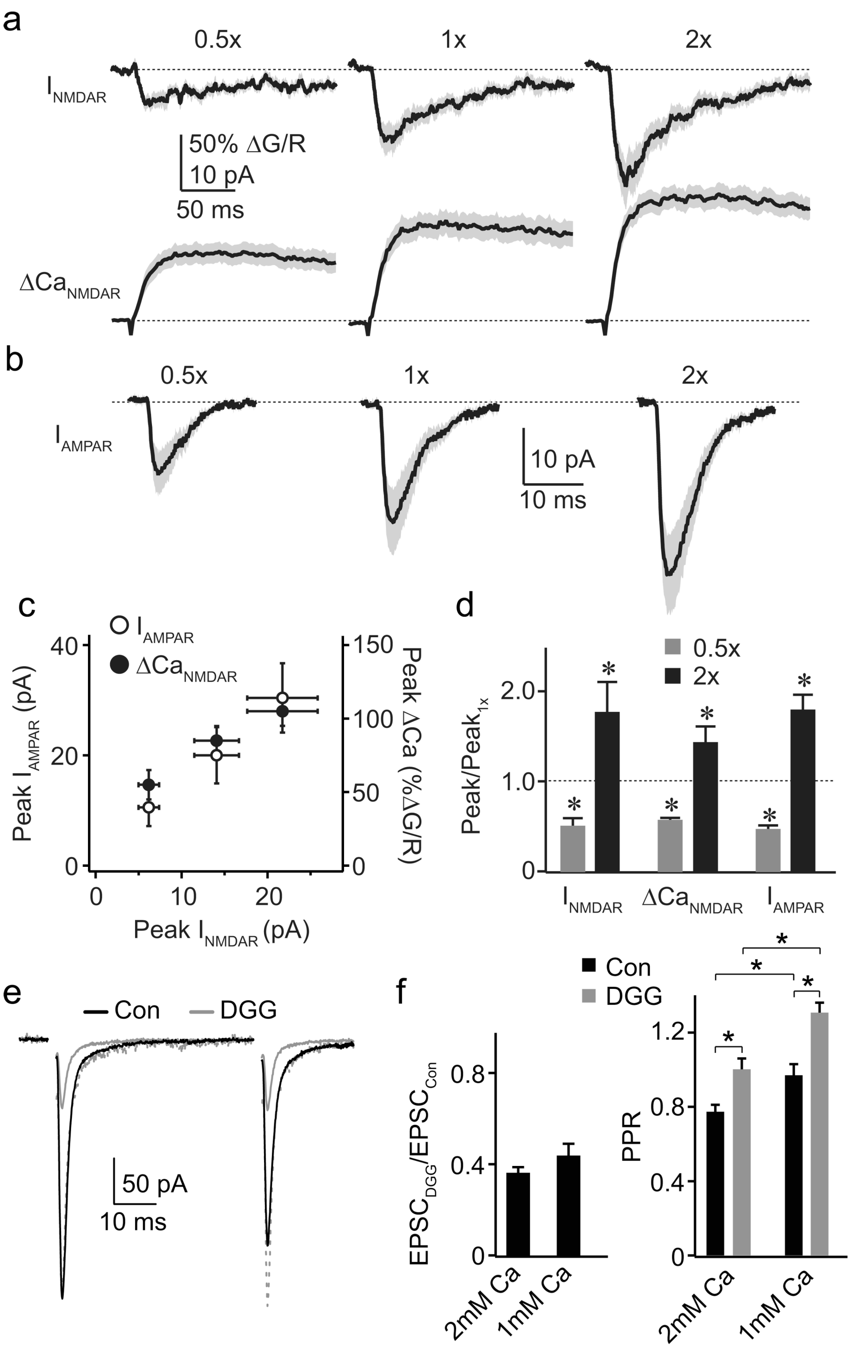

Figure 7. AMPARs and NMDARs are not saturated under basal release conditions

(a) NMDAR-mediated uEPSCs (top traces) and Ca transients (bottom traces) recorded in the presence of the AMPAR antagonist NBQX (10 μM). Responses were measured using standard laser power (1x), calibrated as in Figure 4, and one half (0.5x) and twice (2x) standard power. Solid lines show the average response (n=13 spines), shaded regions are the average response±SEM.

(b) AMPAR-mediated uEPSCs (n=11 spines) recorded in the presence of the NMDAR antagonist CPP (10 μM). Responses to varying laser power are shown as in (a).

(c) Peak AMPAR-mediated currents and peak NMDAR-mediated currents and Ca transients are directly correlated and vary as a function of laser power.

(d) AMPAR- and NMDAR-mediated responses are shown for the 0.5x (gray bars) and 2x conditions (black bars), normalized to the 1x amplitude. Peak response amplitudes were significantly reduced and enhanced by decreasing and increasing laser power, respectively.

(e) AMPAR-mediated EPSCs recorded in the presence of the NMDAR antagonist CPP (10 μM). Responses before (black) and after (gray) application of 2.5 mM γ-DGG are shown. The post-γ-DGG trace is also shown scaled to the baseline amplitude (dashed trace).

(f) *right*, Average EPSC peak relative to baseline following γ-DGG application in normal (2 mM) and reduced (1 mM) [Ca]. *left*, Average PPR before (black) and after (gray) application of γ-DGG under normal and reduced external [Ca].

* indicates a significant difference between conditions ($p<0.05$), corrected for multiple comparisons in (f).

Author Manuscript Author Manuscript Author Manuscript Author Manuscript

Author Manuscript Author Manuscript Author Manuscript Author Manuscript

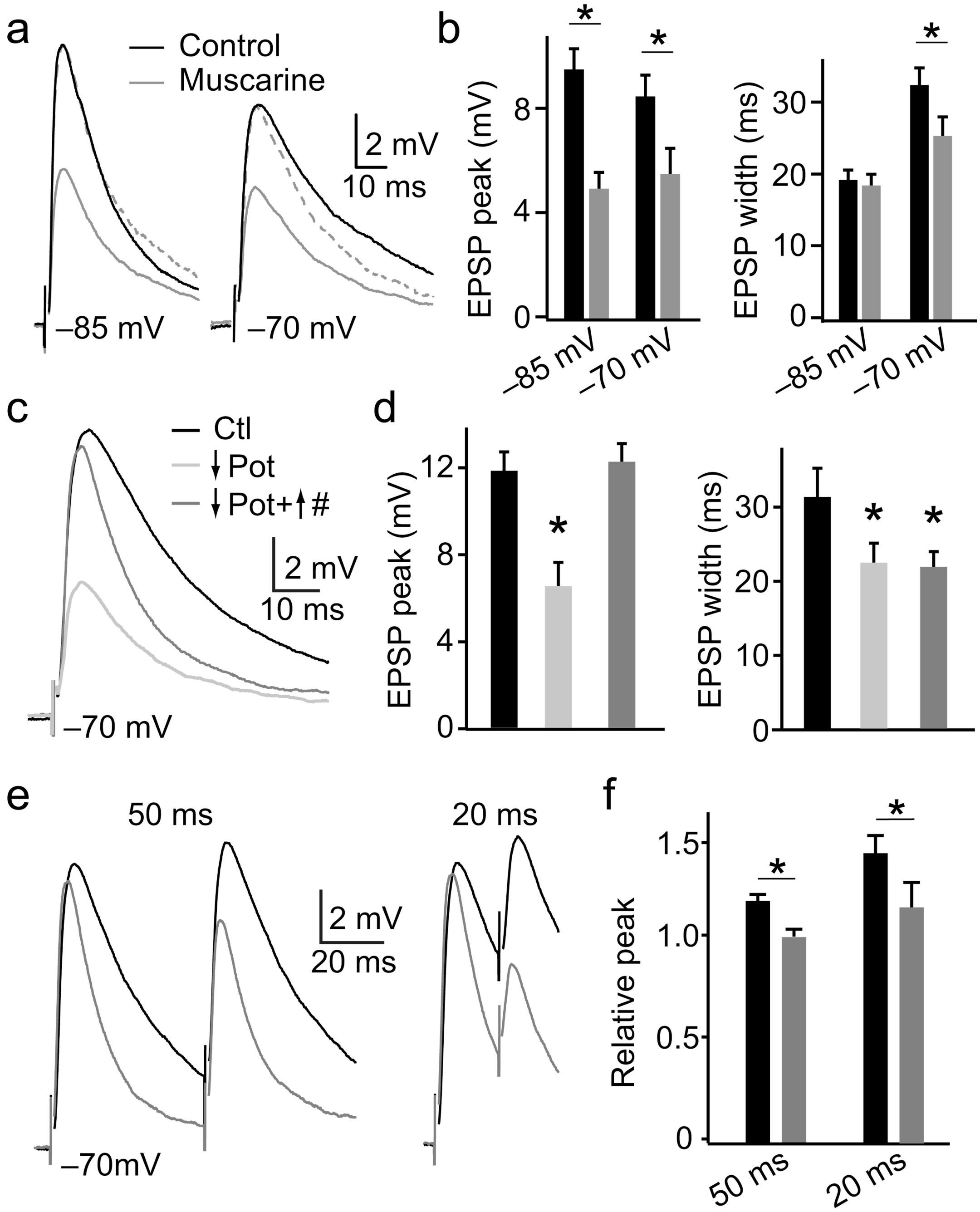

Figure 8. Changes in synaptic potency regulate temporal integration of striatal glutamatergic synapses

(a) EPSPs before (black lines) and after (gray lines) muscarine application for two different MSNs where V_m was held constant at either –85 mV or –70 mV, respectively. The post-muscarine EPSPs scaled to control amplitude are also shown (dashed lines).

(b) Average EPSP peak amplitude (*left*) and width (*right*) in control conditions and after muscarine application for cells held at the indicated V_m.

Author Manuscript Author Manuscript Author Manuscript Author Manuscript

(c) EPSPs recorded in an MSN under control conditions (black), after reducing synaptic potency by co-application of 0.1 μM NBQX and 1.0 μM CPP (light gray), and after subsequently increasing stimulus intensity to increase the number of synapses activated and return the peak EPSP amplitude to control levels (medium gray).
(d) Average EPSP peak amplitude (*left*) and width (*right*) in control conditions, after reducing synaptic potency, and after subsequent increase in the number of activated synapses. Shading as in (c).
(e) Paired EPSPs evoked at either 50 ms (*left*) or 20 ms (*right*) intervals recorded in an MSN under control conditions (black lines) or following reduction in synaptic potency and offsetting increase in stimulus intensity (gray lines).
(f) Average peak amplitude of the second EPSP relative to the first EPSP for 50 and 20 ms intervals, under the same conditions shown in (e).
* indicates a significant difference compared with control conditions ($p<0.05$).